Epifluorescence-based Quantitative Microvasculature Remodeling Using Geodesic Level-Sets and Shape-based Evolution

F. Bunyak[1], **K. Palaniappan**[1], **O. Glinskii**[2,4,5], **V. Glinskii**[6], **V. Glinsky**[3,4,5], and **V. Huxley**[2,4]

1 *Department of Computer Science, University of Missouri-Columbia, Columbia, MO 65211 USA*

2 *Department of Medical Pharmacology and Physiology, University of Missouri-Columbia, Columbia, MO 65211 USA*

3 *Department of Pathology and Anatomical Sciences, University of Missouri-Columbia, Columbia, MO 65211 USA*

4 *National Center for Gender Physiology, University of Missouri-Columbia, Columbia, MO 65211 USA*

5 *Harry S. Truman Memorial Veterans Hospital, Columbia, MO 65201 USA*

6 *Harvard University, Cambridge, MA 02138 USA*

Abstract

Accurate vessel segmentation is the first step in analysis of microvascular networks for reliable feature extraction and quantitative characterization. Segmentation of epifluorescent imagery of microvasculature presents a unique set of challenges and opportunities compared to traditional angiogram-based vessel imagery. This paper presents a novel system that combines methods from mathematical morphology, differential geometry, and active contours to reliably detect and segment microvasculature under varying background fluorescence conditions. The system consists of three main modules: vessel enhancement, shape-based initialization, and level-set based segmentation. Vessel enhancement deals with image noise and uneven background fluorescence using anisotropic diffusion and mathematical morphology techniques. Shape-based initialization uses features from the second-order derivatives of the enhanced vessel image and produces a coarse ridge (vessel) mask. Geodesic level-set based active contours refine the coarse ridge map and fix possible discontinuities or leakage of the level set contours that may arise from complex topology or high background fluorescence. The proposed system is tested on epifluorescence-based high resolution images of porcine dura mater microvasculature. Preliminary experiments show promising results.

I. Introduction

Analysis of vessel characteristics is useful in many medical applications i.e. in quantifying effects of certain drugs or in determining the state of various diseases that cause measurable structural changes in blood vessels such as stenoses and aneurysms [1]. Vessel segmentation is the first step in extraction of features such as diameter, wall profile, volume, surface area, permeability, extrinsic curvature and tortuosity [2], and any further analysis on microvascular networks i.e. registration, bifurcations and crossovers analysis [3], [4]. Given the importance, many recent works focus on vessel segmentation [5]. Most of these work concentrate on

angiogram imaging to characterize retinal, brain, or heart blood vessels. In the proposed system, we focus on segmentation of epifluorescence-based high resolution images of dura mater microvasculature. These images pose unique challenges due to broad range of vessel diameters in close neighborhood (from large arteries and veins to venules and capillaries), leakage of the epifluorescent dye out of the vessels, and non-homogeneous distribution of epifluorescence within the vessels. Leakage makes the segmentation particularly challenging since it smooths the vessel edges and causes nonuniform background fluorescence making intensity based methods difficult to use. This paper presents a novel system that combines methods from mathematical morphology, differential geometry, and active contours to reliably detect and segment microvasculature under varying background fluorescence conditions. The system consists of three main modules: (1) vessel enhancement, (2) shape-based initialization, and (3) level-set based segmentation explored in the following sections.

II. Vessel Enhancement

Vessel enhancement is used to improve vessel segmentation, increasing the separability of vessel and background classes by adjusting nonuniform background fluorescence and by decreasing image noise. The preprocessing step improves the overall performance, but is less crucial for our shape-based initialization and geodesic contour evolution compared to intensity based segmentation approaches, particularly those using intensity thresholding. Three main aspects addressed by vessel enhancement include: (1) sharp intensity changes within the blood vessel caused by localized concentration of epifluorescent dye, (2) smoothly varying nonuniform background fluorescence caused by leakage, and (3) spatially varying image noise. To equalize the background, we use the morphological top-hat operation and adaptive histogram equalization. The top-hat operation (Eq. 1) returns the original image minus its morphological opening.

$$tophat(I) = I - ((I \ominus se) \oplus se)$$
$$(I \ominus se)(s,t) = min\{I(s+x,t+y) + se(x,y)\}$$
$$(I \oplus se)(s,t) = max\{I(s+x,t+y) + se(x,y)\}$$
$$where \ (s+x,t+y) \in D_f \cap (x,y) \in D_{se}$$

(1)

Opening with a structuring element (*se*) larger than the widest vessel provides an estimation of the background fluorescence distribution. Subtracting the opened image from the original image tends to equalize the background. Unlike background subtraction with local mean or median, top-hat operation does not blend vessel intensity into background model and approximates epifluorescent dye leakage better than homomorphic filter that assumes an input signal with multiplicative components. To smooth the localized concentration of epifluorescence within the vessels, we use a second top-hat operation, this time with a structuring element smaller than the narrowest vessel. Image noise and localized concentration of epifluorescent dye along the vessels result in sharp intensity changes and locally jagged intensity ridges. Both shape-based initialization (section III) and geodesic active contours (section IV) involve differentiation and are sensitive to noise. Particularly curvature computation in section III is affected by noise because of the second-order derivatives involved. We use anisotropic diffusion [6] to smooth out noise without blurring the vessel edges. Further information on anisotropic diffusion can be found in [7].

III. Shape-based Initialization

Shape-based initialization produces a coarse vessel mask that is used to initialize the active contour vessel segmentation described in Section IV. Active contour methods are initialization sensitive since evolution of PDEs converge to a local minimum of the energy function. For the

coarse segmentation, shape-based properties are chosen because of their robustness to image contrast and intensity variations. Since vessels produce ridges/creases in the intensity map, we explore ridge-based vessel detection. Various definitions and associated detection methods for ridges/creases can be found in [8]. These methods can be roughly classified as: curvature-based [8], [9], directional derivative-based [8]–[11], and (3) height definitions or Hessian-based [12]–[17]. In this work, ridge detection approaches based on curvatures and Hessian matrix have been used. Principal curvature and directions of a surface L correspond to the eigenvalues $\kappa_1 \geq \ldots \geq \kappa_{n-1}$ and eigenvectors $\xi_1 \geq \ldots \geq \xi_{n-1}$ of the shape operator matrix on the tangent space W defined as Eq. 2 where $\mathbf{I}$ and $\mathbf{II}$ are the first and second fundamental forms and $c = \frac{L_x \times L_y}{|L_x \times L_y|}$ [8].

$$W = \mathbf{I}^{-1}\mathbf{II} = \begin{bmatrix} L_x \cdot L_x & L_x \cdot L_y \\ L_x \cdot L_y & L_y \cdot L_y \end{bmatrix}^{-1} \begin{bmatrix} L_{xx} \cdot c & L_{xy} \cdot c \\ L_{xy} \cdot c & L_{yy} \cdot c \end{bmatrix} \tag{2}$$

Ridges can be defined as local extrema of principal curvatures, where the differentiation is taken in the principal directions [8]. Since computation of eigenvalues, thus individual principal curvatures is expensive, mean curvature H (Eq. 3) is often used to classify a surface patch as as ridge, flat, or valley [8], [9].

$$H = \frac{(\kappa_1 + \kappa_2)}{2} = \frac{trace(W)}{2} = \frac{I_y^2 I_{xx} + I_x^2 I_{yy} - 2I_x I_y I_{xy}}{2(I_x^2 + I_y^2)^{\frac{3}{2}}} \tag{3}$$

Height definition [8] is a generalization of local extrema for real-valued functions of a vector variable. A point x_0 is classified as maximum if $\nabla L(x_0) = 0$ (critical point) and $\mathcal{H}(L(x_0))$ is negative definite (all eigenvalues λ_i are negative). Hessian matrix $\mathcal{H}$ (Eq. 4) describes the second order structure of local intensity variations around each point of the image $L(x, y)$:

$$\mathcal{H} = \begin{bmatrix} L_{xx} & L_{xy} \\ L_{xy} & L_{yy} \end{bmatrix} \tag{4}$$

Table I shows possible orientation patterns based on the value of the eigenvalues $\lambda_{1,2}$ (Eq.5) of the Hessian matrix $\mathcal{H}$.

$$\lambda_{1,2} = \frac{1}{2}(L_{xx} + L_{yy} \pm \sqrt{(L_{xx} - L_{yy})^2 + (2L_{xy})^2}) \tag{5}$$

When the height condition holds (critical points, $\nabla L = 0$), according to the Taylor series expansion and curvature definitions, eigenvalues λ_i and eigenvectors v_i of the Hessian matrix correspond to principal curvatures κ_i and principal directions ξ_i respectively [18]. Eigenvalues and eigenvectors of the Hessian matrix have been used in many medical image processing applications as a ridgeness measure for linear/tubular structure enhancement and detection [12]–[17]. Laplacian, $(\Delta(L) = trace(\mathcal{H}) = \lambda_1 + \lambda_2)$, is a good approximation of the sign of the eigenvalues of the Hessian matrix without the expensive eigenvalue decomposition (particularly for high dimensions). Because of this property, Laplacian or its regularized

version Laplacian of Gaussian have been used in many recent vessel detection papers such as [19]–[21]. In this work, we produce a coarse vessel mask by thresholding $trace(\mathcal{H})$ as below:

$$Mask_{vessel}(x,y)= \begin{cases} 1 & trace(\mathcal{H})<\varepsilon \\ 0 & otherwise \end{cases}$$

(6)

IV. Segmentation Using Geodesic Level-sets with Spatially Adaptive Force

Intensity ridges are good initializations for vessel networks, but because of their local nature, obtained ridge maps may have spurious results or discontinuities, particularly for cases of complex topology (bifurcations, crossings etc.), nonuniform leakage of the fluorescent material), irregular vessel diameters. To refine the ridge-based vessel mask, we propose a spatially adaptive geodesic active contour segmentation, tuned to image differential geometric information (i.e. ridges) as well as edge information.

In level set-based active contour methods, a curve $\mathcal{C}$ is represented implicitly via a Lipschitz function ϕ by $\mathcal{C} = \{(x, y)|\phi(x, y) = 0\}$, and the evolution of the curve is given by the zero-level curve of the function $\phi(t, x, y)$ [22]. We use geodesic active contours [23] where the level set function ϕ is evolved using the speed function,

$$\frac{\partial \phi}{\partial t}=g(\nabla \mathbf{I})(F_c+\mathcal{K}(\phi))|\nabla \phi|+\nabla \phi \cdot \nabla g(\nabla \mathbf{I})$$

(7)

where F_c is a constant, $\mathcal{K}$ is the curvature term Eq. 8, and $g(\nabla \mathbf{I})$ is the edge stopping function, a decreasing function of the image gradient, defined as Eq. 9 in this application.

$$\mathcal{K}=div\left(\frac{\nabla \phi}{|\nabla \phi|}\right)=\frac{\phi_{xx}\phi_y^2 - 2\phi_x\phi_y\phi_{xy}+\phi_{yy}\phi_x^2}{(\phi_x^2+\phi_y^2)^{\frac{3}{2}}}$$

(8)

$$g(\nabla \mathbf{I})=exp(-|\nabla G_\sigma(x,y) * \mathbf{I}(x,y)|)$$

(9)

The constant velocity F_c pushes the curve inwards or outwards depending on its sign. The regularization term $\mathcal{K}$ ensures boundary smoothness. $g(\nabla \mathbf{I})$ is used to stop the curve evolution at vessel boundaries. The geodesic active contours are more robust against nonuniform background fluorescence compared to intensity based approaches such as intensity thresholding or Chan-Vese type minimal variance models [22]. However, since they are designed to evolve until edges, they suffer from early stopping on background edges, and contour leaking across weak boundaries. We overcome the first problem by starting the contour close to the vessels using ridge-based initialization. To reduce the effects of the second problem, we propose a spatially adaptive geodesic active contour approach, where the constant force F_c in Eq. 7 is replaced by the proposed adaptive differential geometric force F_A:

$$F_A(x,y)=c_1 \times (trace(\mathcal{H}(I(x,y)))+c_2)$$

(10)

$trace(\mathcal{H}(I))$ returns positive values for intensity valleys, negative values for intensity ridges, and small absolute values in homogeneous regions with small noise. To obtain F_A, $trace(\mathcal{H}$

(I)) is normalized into the $[-1 : +1]$ range, a constant force c_2 ($0 < c_2 < 1$) is added to ensure expansion in homogeneous regions, and the sum is multiplied with a coefficient c_1 ($c_1 > 0$) that tunes the speed of expansion. In our tests c_1 and c_2 are set to 1 and 0.5 respectively. Using this differential geometric adaptive force F_A instead of a constant balloon force increases the convergence speed on homogeneous regions and decreases contour leaks around weak boundaries. The overall vessel segmentation approach is summarized in Algorithm 1.

V. Results and Analysis

The biological motivaton is to study the influence of hormone treatments on angiogenesis and vasculature remodeling. In an *ex vivo* process, brain dura mater endothelial cells are stained by infusing fluorescently labeled lectin SBA. The epifluorescence images were then acquired with a 10x lens, at 0.56 *μ/pixel* resolution using Laborlux 8 microscope and QICAM digital CCD camera. 100 images from 6 female porcine specimens, three with intact ovary, three with excised ovary were used for characterizing normal microvasculature and OVX case respectively. Figure 1 shows intermediate results for vessel enhancement described in section II and ridgeness measures explored in section III. Top-hat and anisotropic filters are quite effective in correcting the non-uniform background caused by epifluorescent dye leakage and smoothing the jagged edges caused by localized concentration of epifluorescent dye respectively. Compared to Laplacian and λ_1, mean curvature H produces noisier results. As expected, λ_1 and Laplacian produces comparable results, with smoother ridges and less blobs in λ_1. λ_2 shows blob/corner like features. Figure 2 shows results for three cases including original epifluorescence imagery, comparison to the Chan and Vese level-set segmentation results initialized with uniformly distributed disks, and the vessel segmentation mask from our method which is accurate and clearly provides a superior vessel mask. Once an accurate segmentation of the microvasculature is obtained a number of quantitative parameters can be extracted to characterize the morphological and architectural features of terminal microvasulature networks.

VI. Conclusion

The focus of this paper is the novel biomedical application of microvasculature segmentation using epifluorescence imagery of *ex vivo* brain *dura mater* (outermost lining of the brain surface) at very high half-micron per pixel spatial resolution. Previous studies on blood vessel segmentation have typically used angiogram imaging modalities to characterize retinal as well as brain and heart blood vessels. This paper is novel in both the medical imaging epifluorescence modality as well as the tissue vasculature studied. Current approaches to vessel segmentation lead to poor results with epifluorescence imagery. We showed that our new approach using morphology-based background fluorescence correction, differential geometry-based ridge and curvature detection, combined with adaptive geodesic level sets leads to extremely good results for the automatic segmentation of the vasculature regions. The approach is robust to a variety of challenging image conditions including non-uniform spatially varying background fluorescence, leakage of flourescent material outside the vasculature walls, non-homogeneous interior regions of the vessel lumen, with random spatial accumulation of fluorescent material. The proposed segmentation system will be used in characterization of OVX (ovary removed) versus normal cases for studying systemic influence of hormone therapy.

Acknowledgements

References

1. Huang A, Farin GE, Baluch DP, Capco DG. Thin structure segmentation and visualization in three-dimensional biomedical images: A shape-based approach. IEEE Trans on Vis and Comp Graphics 2006;12(1):93–102.

2. Bullitt E, Gerig G, Pizer SM, Lin W, Aylward SR. Measuring tortuosity of the intracerebral vasculature. IEEE Trans Med Imaging 2003;22(9):1163–1171. [PubMed: 12956271]

3. Tsai CL, Stewart CV, Tanenbaum HL, Roysam B. Model-based method for improving the accuracy and repeatability of estimating vascular bifurcations and crossovers from retinal fundus images. IEEE Trans on Inf Tech in Biomed 2004;8(2):122–130.

4. Choe, TE.; Cohen, I. Registration of multimodal fluorescein images sequence of the retina. Proc. IEEE Int. Conf. on Comp. Vision (ICCV'05) Vol. 1; Washington, DC, USA. 2005. p. 106-113.

5. Kirbas C, Quek F. A review of vessel extraction techniques and algorithms. ACM Comput Surv 2004;36(2):81–121.

6. Perona P, Malik J. Scale-space and edge detection using anisotropic diffusion. IEEE Trans on Patt Anal and Mach Intell July;1990 12(7):629–639.

7. Weickert, J. Anisotropic Diffusion in Image Processing. Stuttgart, Germany: ECMI Series, Teubner-Verlag; 1998.

8. Eberly D, Gardner R, Morse B, Pizer S, Scharlach C. Ridges for image analysis. J Math Img Vis 1994;4 (4):353–373.

9. Lopez AM, Lumbreras F, Serrat J, Villanueva JJ. Evaluation of methods for ridge and valley detection. IEEE Trans Pattern Anal Mach Intell 1999;21(4):327–335.

10. Maintz JBA, van den Elsen PA, Viergever MA. Evaluation of ridge seeking operators for multimodality medical image matching. IEEE Trans on Patt Anal and Mach Intell 1996;18(4):353–365.

11. Lindeberg T. Feature detection with automatic scale selection. Int J Comp Vision 1998;30(2):77–116.

12. Sato Y, Nakajima S, Atsumi H, Koller T, Gerig G, Yoshida S, Kikinis R. 3d multi-scale line filter for segmentation and visualization of curvilinear structures in medical images. Medical Image Analysis june;1998 2(2):143–168. [PubMed: 10646760]

13. Lorenz, C.; Carlsen, I-C.; Buzug, TM.; Fassnacht, C.; Weese, J. Proceedings of CVRMed-MRCAS '97. London, UK: Springer-Verlag; 1997. Multi-scale line segmentation with automatic estimation of width, contrast and tangential direction in 2d and 3d medical images; p. 233-242.

14. Frangi AF, Niessen WJ, Vincken KL, Viergever MA. Multiscale vessel enhancement filtering. Lecture Notes in Computer Science - MICCAI98 1998;1496:130–137.

15. Krissian K, Malandain G, Ayache N, Vaillant R, Trousset Y. Model-based detection of tubular structures in 3d images. Computer Vision Image Understanding 2000;80(2):130–171.

16. Staal J, Abràmoff MD, Niemeijer M, Viergever MA, van Ginneken B. Ridge-based vessel segmentation in color images of the retina. IEEE Trans Med Imaging 2004;23(4):501–509. [PubMed: 15084075]

17. Zhou, J.; Chang, S.; Metaxas, D.; Axel, L. Vessel boundary extraction using ridge scan-conversion deformable model. IEEE Int. Symp. Biomed. Img.: Macro to Nano; Apr. 2006; p. 189-192.

18. Bronshtein, IN.; Semendyayev, KA. Handbook of mathematics. 3. London, UK: Springer-Verlag; 1997. ch. Chapter 4.3.

19. Zana F, Klein JC. Segmentation of vessel-like patterns using mathematical morphology and curvature evaluation. IEEE Trans on Image Proces 2001;10(7):1010–1019.

20. Fang B, Hsu W, Lee M. Reconstruction of vascular structures in retinal images. ICIP03 2003(II): 157–160.

21. Vermeer KA, Vos FM, Lemij HG, Vossepoel AM. A model based method for retinal blood vessel detection. Computers in Biology and Medicine 2004;34(3):209–219. [PubMed: 15047433]

22. Chan T, Vese L. Active contours without edges. IEEE Trans Image Process Feb;2001 10(2):266–277. [PubMed: 18249617]

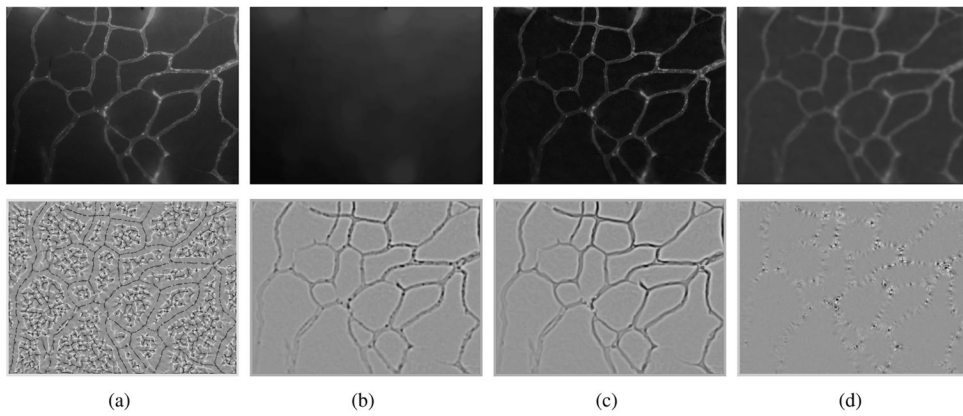23. Caselles V, Kimmel R, Sapiro G. Geodesic active contours. Int Journal of Computer Vision 1997;22 (1):61–79.

Fig. 1.
Row 1:Vessel enhancement(a) Original intensity map, (b) background estimation (opening), (c) background adjusted image (top-hat filter), (d) smoothed image (anisotropic diffusion filter + sqrt transformation). Row 2: Ridgeness measures(a) Mean curvature H, (b) Laplacian, (c) λ_1, (d) λ_2 ($|\lambda_1| \geq |\lambda_2|$). Images in second row have been obtained by shifting the actual values. Dark: negative values, bright: positive values.
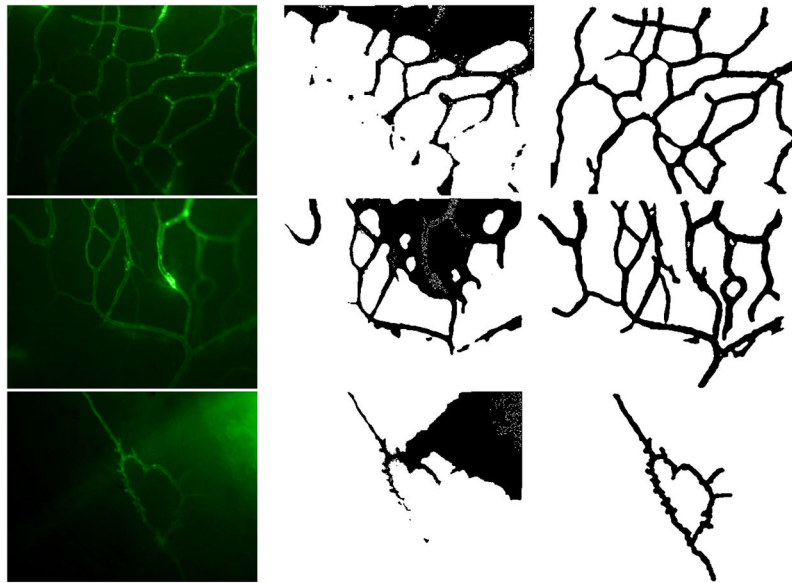
Fig. 2.
Comparison of the segmentation results. Column 1: original epifluorescence imagery for three distinct cases; column 2: Chan and Vese level-set segmentation [22] initialized with uniformly distributed disks; column 3: vessel mask from the proposed method.

TABLE I

Possible orientation patterns based on the value of eigenvalues λ_1, λ_2 (H=high, L=low, $|\lambda_1| \geq |\lambda_2|$) [14].

λ_1	λ_2	orientation pattern
L	L	Flat or Noise no preferred direction
H−	L	Bright tubular structure
H+	L	Dark tubular structure
H−	H−	Bright blob-like structure
H+	H+	Dark blob-like structure

Algorithm 1

Vessel Segmentation

Require: Enhanced epifluorescence-based vessel image **I**

Ensure: Background-Vessel mask $\text{Mask}_{\text{Vessel}}$ (1:Vessel, 0:BG)

1: $\mathcal{H}(\text{I}) \leftarrow Hessian(\mathbf{I})$
2: $g(\nabla\mathbf{I}) = exp(-|\nabla G_\sigma(x, y) * \mathbf{I}(x, y)|)$ // Edge stopping function
3: $F_A(x, y) = c_1 \times (\text{trace}(\mathcal{H}(\mathbf{I}(x, y))) + c_2)$ // Differential geometric adaptive force
4: $\text{Mask}_{\text{ridge}}(x, y) \leftarrow$ Initialize ridge mask
5: $\text{Mask}_{\text{ridge}}(\text{trace}(\mathcal{H}) < \varepsilon) \leftarrow 1$ // Set ridge (vessel) pixels to 1
6: $\text{Mask}_{\text{ridge}} = \text{Mask}_{\text{ridge}} \oplus se$ // Dilate ridges
7: $\phi = SignedDist(\text{Mask}_{\text{ridge}})$ //Initialize ϕ using signed distance transform of $\text{Mask}_{\text{ridge}}$; $\text{Mask}_{\text{ridge}} == 0 \rightarrow \phi > 0$
8: **while** stopping/convergence condition not met **do**
9:    Evolve ϕ using $g(\nabla\mathbf{I})$ and spatially adaptive force F_A.
10: **end while**
11: $\text{Mask}_{\text{Vessel}}(x, y) \leftarrow 0$; $\text{Mask}_{\text{Vessel}}(\phi < 0) \leftarrow 1$ // 1: Vessel, 0:BG